Earthline Journal of Mathematical Sciences
E-ISSN: 2581-8147
Volume 11, Number 1, 2023, Pages 115-143
https://doi.org/10.34198/ejms.11123.115143

Effects of Temperature Fluctuations on Darcy-Forchheimer Flow of Oil-Based Nanofluid with Activation Energy and Velocity Slip

Christian John Etwire[1,*], Ibrahim Yakubu Seini[2], Rabiu Musah[3] and Oluwole Daniel Makinde[3]

[1] Department of Mathematics, School of Mathematical Sciences, CK Tedam University of Technology and Applied Sciences, P.O. Box 24, Navrongo, UER, Ghana
e-mail: jecpapa@yahoo.com

[2] Department of Mechanical & Industrial Engineering, School of Engineering, University for Development Studies, P.O. Box 1882, Tamale, Ghana
e-mail: dr.yseini@uds.edu.gh

[3] Department of Physics, School of Engineering, University for Development Studies, P.O. Box 1882, Tamale, Ghana
e-mail: mrabiu@uds.edu.gh

[4]Faculty of Military Science, Stellenbosch University, Private Bag X2, Saldanha 7395, South Africa
e-mail: makinded@gmail.com

Abstract

The effects of fluctuating temperature on Darcy-Forchheimer flow of oil-based nanofluid with activation energy and velocity slip has been analyzed. Similarity transformation was used to transform the governing partial differential equations into coupled nonlinear ordinary differential equations and solved numerically with the aid of the fourth order Runge-Kutta algorithm with a shooting technique. Results for the embedded parameters controlling the flow dynamics have been tabulated and illustrated graphically. The slip velocity parameter was found to enhance the Nusselt number but depleted both the skin friction coefficient and Sherwood number while the local inertial was noted to increase both the skin friction coefficient and Sherwood number but diminishes the Nusselt number. These results indicate that the velocity slip parameter and local inertial coefficient can be used to control flow characteristics in industrial and engineering systems.

Received: July 27, 2022; Accepted: September 7, 2022; Published: September 14, 2022

2020 Mathematics Subject Classification: 76W05.

Keywords and phrases: Darcy-Forchheimer, velocity slip, dielectric, temperature jump.

*Corresponding author

Nomenclature

(x, y) = Cartesian coordinates
(u, v) = Velocity components directed in the x and y axes
T_f = Temperature of hot fluid
T_∞ = Free-stream temperature of nanofluid
T_w = Temperature of the sheet
T = Temperature of nanofluid
k_f = Oil Thermal Conductivity
k_s = Nanoparticle Thermal Conductivity
c_p = Specific heat at constant pressure
k' = Permeability of the porous media
K^* = Permeability parameter
K_r^2 = Chemical reaction rate constant
K_* = Stefan Boltzmann constant
C_b = Drag coefficient
n = Fitted rate constant
D_B = Brownian diffusion coefficient
Ea = Activation energy
F = Inertial coefficient for the porous media
D = Local inertial coefficient
H = Velocity slip parameter
h_f = Heat transfer coefficient
Pr = Prandtl number
C_f = skin-friction coefficient
Re = Reynolds number
Nu = Nusselt number
q_w =Wall heat flux
q_m =Wall mas flux
Le = Lewis number
Ec = Eckert number
U_∞ = Free stream velocity of nanofluid
S = Suction parameter
C = Concentration of nanofluid
C_∞ = Free-stream concentration of nanofluid
C_w = Concentration of the sheet
M = Temperature jump parameter
T_m = Mean temperature of the nanofluid
Sh = Sherwood number

Symbols

η = Dimensionless Variable
τ_w = Wall shear stress
μ_{nf} = Dynamic viscosity of nanofluid
υ_f = Oil Kinematic Viscosity
ρ_{nf} = Density of nanofluid
α = Thermal diffusivity of oil
ρ_f = Density of oil
ρ_s = Density of nanoparticles
ψ = Stream function
θ = Dimensionless temperature
γ = Reaction rate parameter
$\phi(\eta)$ = Dimensionless concentration
σ_T = temperature difference parameter
β = Chemical reaction rate parameter
ϕ = Solid volume fraction of nanoparticles
$(\rho c_p)_{nf}$ = Heat capacitance of nanofluid

1. Introduction

Porous media is encountered in many industrial and engineering flow processes. It is encountered in petrol-chemical processes by engineers, geoscientists, biologists, biophysicists, and material scientists within a framework of poromechanics. It has significant application in the modeling of blood flow through the myocardium, the movement of water in geothermal reservoirs, nuclear waste repository, underground spreading of chemical waste and recovery of oil from reservoirs. In these applications, the Darcy Forchheimer model is employed due to its robustness over the Darcian model. The effects of viscous dissipation and chemical reaction on a mixed convection flow of Darcy-Forchheimer through saturated porous media has been examined and reported by many researchers [1-4] who reported that both the thermal and concentration profiles are enhanced with the inertial parameter in magnetohydrodynamic (MHD) mixed convection flow in porous media. The Darcy-Forchheimer nanofluid flow with varying flow dynamics has been reported [5-10].

Activation energy plays a pivotal role in ensuring desired end product in many industrial and engineering processes. Ramzan *et al.* [11] observed that the activation energy parameter increases the heat transfer rate but allows the rate of mass transfer in a buoyancy induced radiation in a micropolar nanofluid flow with double stratification. The activation energy and chemical reaction effects on MHD nanofluid flow across a vertical surface [12] have been reported. Kumar *et al.* [13] employed an improved heat diffusion scheme with the binary chemical reaction to investigate the activation energy requirement for Carreau fluid flow acted on by a transverse magnetic field. A numerical study of Darcy-Forchheimer nanofluid flow caused by a disk rotating in a chemical reacting fluid was reported by Asma *et al.* [15]. The effects of activation energy and entropy generation on mixed convection flow of viscous nanofluid of higher order chemically reacting species [16, 17] has been discussed.

The above studies assumed no-slip condition but there are engineering phenomena such as oil emulsion where slip condition is eminent. Heat transfer at slip surfaces is influenced by the rise in temperature. Rashidi and Mehr [18] analyzed the effects of temperature jump and velocity slip on the entropy generation in MHD flow around a rotating disk. Singh and Makinde [19] noted the positive effects of slip parameter on the velocity of flow whilst the opposite trend is observed for temperature jump parameter in a mixed convection flow with free stream conditions. Adesanya [20] examined the heat generated by free convective flow through a permeable channel with velocity slip and

temperature jump. The effects of velocity slip and temperature jump on the peristaltic Jeffrey fluid flow with a Newtonian fluid has been reported [21]. Opanuga *et al.* [22] discussed the effects of ion-slip and hall current on the couple stress fluid with entropy generation, temperature jump and slip velocity. Titiloye *et al.* [23] analyzed the numerical solution for an oscillatory and radiating MHD flow through a channel experiencing velocity slip with internal heat generation. Gangadhar et al. [24] used non-Fourier Cattaneo-Christov heat flux to investigate the effects of velocity slip and thermal jump on the flow of Maxwell fluids. The MHD flow of second-order nanofluid with homogeneous-heterogeneous chemical reactions in a porous medium with velocity slip [25] and the impact of nonlinear velocity slip and temperature jump on the heat transfer potential of nanofluid flow of non-Newtonian nature in a perpendicular acting magnetic field [26] has been studied. The effects of viscoelasticity on oil-based nanofluid under various operating conditions has been reported extensively by Etwire *et al.* [27-29] and the references therein

The present communication analyzes the impact of fluctuating temperature and velocity slip on Darcy-Forchheimer flow of oil-based nanofluid with activation energy in a porous media. The study finds its relevance in the automobile and tribological industries as the surfaces of engine parts exhibit slip conditions. It is imperative to cool these parts to avoid localized welding and improve upon its performance. The remainder of the paper is presented as follows: the mathematical representation of the model is presented in Section 2. In Section 3, the similarity transformation is outlined. Section 4 outlines the computation approach. The graphical and numerical results are illustrated and discussed in Section 5. Section 6 presents conclusion of the study.

2. Mathematical Model

An incompressible dielectric and chemically reacting oil based nanofluid which contains copper oxide (CuO) particles and flowing steadily over an exponentially stretching sheet embedded in a porous media with activation energy has been considered. The x-axis is assumed to act along the direction of the sheet whilst the y-axis is assumed perpendicular to the flow (Figure 1). A stream of cold oil-based nanofluid at the free stream temperature T_∞ moves over the upper surface of the sheet with a uniform free stream velocity U_∞ and free stream concentration C_∞ while the surface of the plate experiences slip and is heated by convection from a hot fluid with fluctuating temperature $T_f\left(T_w = T_\infty + T_0 e^{\frac{x}{2L}} + Q_2 \frac{\partial T}{\partial y}\right)$ and concentration $C_W = C_\infty + C_0 e^{\frac{x}{2L}}$. The exponentially

stretching slippery surface has a velocity defined as $u_w(x) = U_0 e^{\frac{x}{L}} + Q_1 \frac{\partial u}{\partial y}$ acting in the direction of the x-axis and $v_w = -V$ acting in the direction of the y-axes.

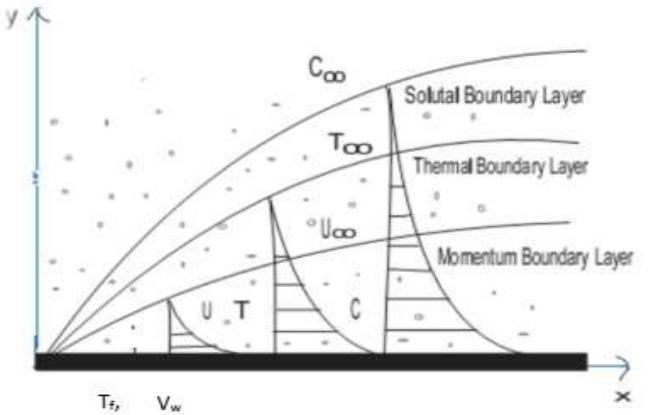

Figure 1: Flow diagram of problem.

In the modeling process, the nanoparticles and the fluid medium are taken to be at thermal equilibrium. The changes in the density of the nanofluid are accounted for by using the Boussinesq approximation. The equations modeling the flow are developed as follows;

$$\frac{\partial u}{\partial x} + \frac{\partial v}{\partial y} = 0, \tag{1}$$

$$u\frac{\partial u}{\partial x} + v\frac{\partial u}{\partial y} = \frac{\mu_{nf}}{\rho_{nf}}\frac{\partial^2 u}{\partial y^2} - \frac{\mu_{nf}}{\rho_{nf}k'}u - Fu^2, \tag{2}$$

$$u\frac{\partial T}{\partial x} + v\frac{\partial T}{\partial y} = \frac{k_{nf}}{(\rho c_p)_{nf}}\frac{\partial^2 T}{\partial y^2} + \frac{\mu_{nf}}{(\rho c_p)_{nf}}\left(\frac{\partial u}{\partial y}\right)^2, \tag{3}$$

$$u\frac{\partial C}{\partial x} + v\frac{\partial C}{\partial y} = D_B\frac{\partial^2 C}{\partial y^2} - K_r^2(C - C_\infty)\left(\frac{T}{T_\infty}\right)^n e^{\left(-\frac{Ea}{K_* T}\right)}, \tag{4}$$

where u and v represent the x and y components of velocities respectively, μ_{nf} is the dynamic viscosity of the nanofluid, k_{nf} is the thermal conductivity of the nanofluid, ρ_{nf} is the density of the nanofluid, k' is the permeability of the porous media, $F = \frac{C_b}{x\sqrt{k'}}$ is the inertial coefficient for the porous media, Q_1 is the velocity slip factor, C_b is the drag coefficient, Q_2 is the temperature jump factor, T is the nanofluid temperature, $(\rho c_p)_{nf}$ is

heat capacitance of the nanofluid, C is concentration of the nanofluid and D_B is Brownian diffusion coefficient. The term $K_r^2(C-C_\infty)\left(\frac{T}{T_\infty}\right)^n e^{\left(-\frac{Ea}{K_*T}\right)}$ in equation (4) represents Arrhenius expression where K_r^2 is chemical reaction rate constant, Ea is the activation energy, $K_* = 8.61 \times 10^{-5}$eV/K is Stefan Boltzmann constant and n is fitted rate constant whose value is in the range specified as; $-1 < n < 1$.

On the surface of the plate, $y = 0$ and the boundary conditions specified as:

$$u(x,0) = U_0 e^{\frac{x}{L}} + Q_1\frac{\partial u}{\partial y}, \quad v(x,0) = -v_w, \quad T(x,0) = T_w(x,0) = T_\infty + T_0 e^{\frac{x}{2L}} + Q_2\frac{\partial T}{\partial y},$$

$$C(x,0) = C_w(x,0) = C_\infty + C_0 e^{\frac{x}{2L}}. \tag{5}$$

The boundary conditions of the oil-based nanofluid at the far location from the plate as $y \to \infty$ are;

$$u(x,\infty) \to 0, \quad T(x,\infty) \to T_\infty, \quad C \to C_\infty. \tag{6}$$

The properties of the nanofluid with spherical sized nanoparticles are defined [30, 31] as

$$\rho_{nf} = (1-\varphi)\rho_f + \varphi\rho_s, \tag{7}$$

$$\mu_{nf} = \frac{\mu_f}{(1-\varphi)^{2.5}}, \tag{8}$$

$$\left(\rho c_p\right)_{nf} = (1-\varphi)\left(\rho c_p\right)_f + \varphi\left(\rho c_p\right)_s, \tag{9}$$

$$k_{nf} = \frac{\left(k_s + 2k_f\right) - 2\varphi\left(k_f - k_s\right)}{\left(k_s + 2k_f\right) + \varphi\left(k_f - k_s\right)}k_f, \tag{10}$$

where ρ_f and ρ_s represent the reference densities of oil and CuO nanoparticles respectively, φ is the solid volume fraction of the nanoparticles, k_f and k_s are the thermal conductivities of the base fluid and CuO nanoparticles respectively and c_p is the specific heat at constant pressure and $(\rho c_p)_{nf}$ is the capacitance of the oil-based nanofluid.

3. Similarity Transformations

To achieve a similarity solution of equations (1)-(6), an independent dimensionless variable, η, a stream function, ψ, are defined in terms of a dependent variable $f(\eta)$, a dimensionless temperature $\theta(\eta)$ and a dimensionless concentration $\phi(\eta)$ as;

$$\eta = y\sqrt{\frac{U_0}{2L\upsilon_f}}e^{\frac{x}{2L}},\ \ \psi = \sqrt{2L\upsilon_f U_0}f(\eta)e^{\frac{x}{2L}},\ \ \theta(\eta) = \frac{T-T_\infty}{T_0 e^{\frac{x}{2L}}},\ \ \phi(\eta) = \frac{C-C_\infty}{C_0 e^{\frac{x}{2L}}}, \tag{11}$$

Defining the stream function, $\psi(x,y)$ in the usual way satisfies the continuity equation automatically. Thus;

$$u = \frac{\partial\psi}{\partial y} \quad \text{and} \quad v = -\frac{\partial\psi}{\partial x}. \tag{12}$$

Substituting the relevant terms in the required forms into equations (2)-(6) yields the coupled nonlinear differential equations as;

$$\frac{\rho_f}{(1-\varphi)^{2.5}\left((1-\varphi)\rho_f + \varphi\rho_s\right)}f'''(\eta) - 2(1+D)\left(f'(\eta)\right)^2 + f(\eta)f''(\eta)$$

$$-\frac{2\rho_f k^*}{(1-\varphi)^{2.5}\left((1-\varphi)\rho_f + \varphi\rho_s\right)}f'(\eta) = 0, \tag{13}$$

$$\frac{\left(k_s+2k_f\right)-2\varphi\left(k_f-k_s\right)}{\left(k_s+2k_f\right)+\varphi\left(k_f-k_s\right)}\theta''(\eta)$$

$$+\frac{(1-\varphi)\left(\rho c_p\right)_f + \varphi\left(\rho c_p\right)_s}{\left(\rho c_p\right)_f}Pr\left(f(\eta)\theta'(\eta) - f'(\eta)\theta(\eta)\right)$$

$$+\frac{Pr\,E\,c}{(1-\varphi)^{2.5}}\left(f''(\eta)\right)^2 = 0, \tag{14}$$

$$\phi''(\eta) - Le\,Pr\,f'(\eta)\phi(\eta) + Le\,Pr\,f(\eta)\phi'(\eta)$$

$$-2Le\,Pr\,\beta\,\phi(\eta)(\sigma_T\theta(\eta)+1)^N e^{\left(-\frac{E}{(\sigma_T\theta(\eta)+1)}\right)} = 0, \tag{15}$$

subject to the boundary conditions;

$$f'(0) = 1 + Hf''(0), f(0) = S, \theta(0) = 1 + M\theta'(0), \phi(0) = 1, \tag{16}$$

$$f'(\infty) \to 0, \theta(\infty) \to 0, \phi(0) \to 0, \tag{17}$$

The prime symbol denotes differentiation with respect to η, $k^* = \frac{L\upsilon_f e^{-\frac{x}{L}}}{U_0 k'}$ is the permeability parameter, $S = \frac{V_w}{\sqrt{\frac{\upsilon_f U_0}{2L}}e^{\frac{x}{2L}}}$ is the suction parameter, $H = Q_2\sqrt{\frac{U_0}{2L\upsilon_f}}e^{\frac{x}{2L}}$ is the

velocity slip parameter, $D = \frac{LC_b}{x\sqrt{k'}}$ is the local inertial coefficient, $M = Q_2\sqrt{\frac{U_0}{2L\upsilon_f}}e^{\frac{x}{2L}}$ is the local temperature jump parameter, $\beta = \frac{LK_r^2}{U_0 e^{\frac{x}{L}}}$ is the local reaction rate parameter, $Le = \frac{\alpha_f}{D_B}$ is the Lewis number, $\sigma_T = \frac{T_0 e^{\frac{x}{2L}}}{T_\infty}$ represents the local temperature difference parameter, $E = \frac{Ea}{k_f T_\infty}$ represents the activation energy parameter. The local skin-friction coefficient (C_f), Nusselt number (Nu) and Sherwood number (Sh) are the main parameters of engineering applications considered in the study. They are respectively defined as;

$$C_f = \frac{\tau_w}{\rho_f u_w^2}, \quad Nu = \frac{xq_w}{k_f(T_w - T_\infty)}, \quad Sh = \frac{xq_m}{D_B(C_w - C_\infty)}, \tag{18}$$

where τ_w is the wall shear stress, q_w denotes the wall heat flux and q_m denotes the wall mass flux which are respectively defined by;

$$\tau_w = \mu_{nf}\left.\frac{\partial u}{\partial y}\right|_{y=0}, \quad q_w = -k_{nf}\left.\frac{\partial T}{\partial y}\right|_{y=0}, \quad q_m = -D_B\left.\frac{\partial C}{\partial y}\right|_{y=0}. \tag{19}$$

Substituting equation (19) into equation (18) yields;

$$C_f = \frac{\mu_f}{(1-\varphi)^{2.5}}\sqrt{\frac{1}{2Re_x}}\, f''(0), \tag{20}$$

$$Nu = -\frac{x}{L}\frac{(k_s + 2k_f) - 2\varphi(k_f - k_s)}{(k_s + 2k_f) + \varphi(k_f - k_s)}\sqrt{\frac{1}{2}Re_x}\,\theta'(0), \tag{21}$$

$$Sh = -\frac{x}{L}\sqrt{\frac{1}{2}Re_x}\,\phi'(0), \tag{22}$$

where, $Re_x = \frac{U_0 e^{\frac{x}{L}} L}{\upsilon_f}$ is the local Reynolds number.

4. Computational Approach

The nonlinear flow equations are reduced to a first system order ordinary differential equations by letting;

$$f = x_1, \; f' = x_2, \; f'' = x_3, \; f''' = x_4, \quad \theta = x_5, \quad \theta' = x_6, \quad \theta'' = x_7,$$

$$\phi = x_8, \quad \phi' = x_9, \quad \phi'' = x_{10}. \tag{23}$$

Substituting equations (23) into equations (13)-(17) yields the required system of equations as;

$$f'(\eta) = x_1' = x_2,$$

$$f''(\eta) = x_2' = x_3,$$

$$f'''(\eta) = x_3' = x_4 = \frac{(1-\varphi)^{2.5}\left((1-\varphi)\rho_f + \varphi\rho_s\right)}{\rho_f} \times \left(\frac{2\rho_f k^*}{(1-\varphi)^{2.5}\left((1-\varphi)\rho_f + \varphi\rho_s\right)} x_2 + 2(1+D)x_2^2 - x_1 x_3\right),$$

$$\theta'(\eta) = x_5' = x_6,$$

$$\theta''(\eta) = x_6' = x_7 = -\frac{\left(k_s + 2k_f\right) + \varphi\left(k_f - k_s\right)}{\left(k_s + 2k_f\right) - 2\varphi\left(k_f - k_s\right)} \times \left(\frac{(1-\varphi)\left(\rho c_p\right)_f + \varphi\left(\rho c_p\right)_s}{\left(\rho c_p\right)_f} Pr(x_1 x_6 - x_2 x_5) + \frac{Pr\, E\, c}{(1-\varphi)^{2.5}} x_3^2\right),$$

$$\phi' = x_8' = x_9$$

$$\phi''(\eta) = x_9' = x_{10} = LePrx_2 x_8 - LePrx_1 x_9 + 2Le\, Pr\, \beta\, x_8(\sigma_T x_5 + 1)^N e^{\left(-\frac{E}{(\sigma_T x_5 + 1)}\right)} \tag{24}$$

subject to the boundary conditions;

$$x_2 = 1 + Hx_3,\ x_1 = S,\ x_5 = 1 + Mx_6,\ \ x_8 = 1,\ \ x_2 = J,\ \ x_5 = K,\ \ x_8 = L. \tag{25}$$

The unknowns; J, K and L are obtained by employing the shooting technique. The fourth order Runge-Kutta integration scheme is used to solve the resulting initial value problem.

5. Results and Discussions

The flow parameters considered in this study are the permeability parameter (K^*), suction parameter (S), velocity slip parameter (H), local inertial coefficient (D), temperature jump parameter (M), local chemical reaction parameter (β), Lewis number (Le), local temperature difference parameter (σ_T), activation energy parameter (E), solid

volume fraction of CuO nanoparticles (φ), fitted rate parameter (N), Prandtl number (Pr) and Eckert number (Ec). The thermophysical properties of oil and CuO nanoparticles at room temperature are presented in Table 1.

Table 1: Thermophysical properties of oil and nanoparticles.

Physical property	C_p '[J/kgK]'	ρ '[Kg/m^3]'	k '[W/mK]'
Oil	1670	920	0.138
CuO	540	6510	18

5.1. Numerical results

The present model's results for the Nusselt number represented by ($-\theta'(0)$) was compared with the work of Bidin and Nazar [32] for varying Prandtl number (Pr) and Eckert number (Ec) when $D = K^* = S = H = M = N = E = \beta = Le = \varphi = \sigma_T = 0$ in the case of non-convective flow. The agreement of the results of the model up to three decimal places validates it. The comparison is depicted in Table 2.

Table 2: Computations showing comparison with Bidin and Nazar [32].

	Bidin and Nazar [32]		***Present Work***	
	$Ec = 0$	$Ec = 0.9$	$Ec = 0$	$Ec = 0.9$
Pr	$-\theta'(0)$	$-\theta'(0)$	$-\theta'(0)$	$-\theta'(0)$
1	0.9547	0.5385	0.9548	0.5386
2	1.4714	0.7248	1.4715	0.7248
3	1.8691	0.8301	1.8691	0.8301

The effect of the flow parameters on the skin friction coefficient ($-f''(\theta)$), Nusselt number ($-\theta'(0)$) and Sherwood number ($-\phi'(0)$) for CuO-oil based nanofluid are presented in Table 3. It can be observed that the intensity of the activation energy has no effect on both the skin friction coefficient and the rate of heat transfer. This however depletes the Sherwood number due to the deteriorating convective mass transfer rate of the nanofluid at the surface of the plate. In addition, the Lewis number, the chemical reaction rate parameter and fitted rate parameter have no influence on both the skin friction coefficient and the rate of heat transfer. They however enhanced the rate of mass transfer due to depleting mass diffusion rate. A hike in the velocity slip parameter increased the Nusselt number but degraded both the skin friction coefficient and Sherwood number due to the convective heat transfer rate of the nanofluid at the surface

of the plate. Furthermore, the rise in the local inertial coefficient causes both the skin friction coefficient and Sherwood number to increase but depleted the Nusselt number. The temperature jump parameter did not influence the skin friction coefficient but decreased both the Nusselt and Sherwood numbers. A reverse trend was noted with the Prandtl number although it did not also affect the skin friction coefficient. The suction parameter was seen to enhance the skin friction coefficient, Nusselt number and Sherwood number whilst the permeability parameter only increased the skin friction coefficient. Also, a rise in the Eckert number leads to a reduced rate of heat and mass transfers. The Eckert number physically enhances the heat transfer potential of the nanofluid but the fluctuating temperature counteracts its effects. The solid volume fraction of CuO nanoparticles enhanced the Sherwood number but decayed both the magnitudes of the skin friction coefficient and the Nusselt number.

Table 3: Computation showing $(-f''(0)), (-\theta'(0))$ and $(-\phi'(0))$ for different parameter values.

E	L	σ_T	β	N	H	D	M	Pr	S	K^*	Ec	ϕ	$-f''(0)$	$-\theta'(0)$	$-\phi(0)$
0.1	0.1	0.1	0.1	0.1	0.2	0.1	0.1	100	0.1	0.1	0.1	0.1	1.132875	5.441198	3.901435
0.3													1.132875	5.441198	3.876759
	0.2												1.132875	5.441198	6.025879
	0.3												1.132875	5.441198	7.815720
		0.3											1.132875	5.441198	3.902332
		0.5											1.132875	5.441198	3.903177
			0.4										1.132875	5.441198	4.290918
			0.7										1.132875	5.441198	4.642234
				0.2									1.132875	5.441198	3.901673
				0.3									1.132875	5.441198	3.901912
					0.4								0.883279	5.504625	3.641256
					0.6								0.729147	5.516257	3.455451
						0.2							1.155871	5.419418	3.885049
						0.3							1.177894	5.365377	3.869293
							0.3						1.132875	2.456604	3.901293
							0.5						1.132875	1.586423	3.901252
								200					1.132875	6.412180	6.025654
								300					1.132875	6.916354	7.815304
									0.3				1.201052	6.862087	5.263021
									0.5				1.272709	7.641883	6.806491
										0.2			1.168974	5.398613	3.873400
										0.3			1.203445	5.357156	3.846351
											0.4		1.132875	3.540894	3.901959
											0.7		1.132875	1.640590	3.902470
												0.2	1.142167	5.075534	3.894532
												0.3	1.110073	4.705408	3.918672

5.2. Graphical results

The effects of various thermophysical parameters on the velocity, temperature and concentrations profiles are illustrated in graphical forms and discussed.

5.2.1. Velocity profiles

The velocity profiles are illustrated in Figures 2-6. Figure 2 depicts the effect of the local inertial coefficient on the velocity profile. It is noted in the Figure that increasing the local inertial coefficient decayed the velocity of the nanofluid within the boundary layer. A rise in the local inertial coefficient corresponds to an increase in the drag coefficient which depletes the momentum boundary layer thickness. Similar trends were seen in Figures 3-5 as the velocity slip, permeability and suction parameters were increased. An enhancement in these parameters strengthens the resistive forces of the flow which weakens the momentum boundary thickness. However, it is observed in Figure 6 that increasing the magnitude of the solid volume fraction of CuO nanoparticles enhanced the velocity of the nanofluid. Physically, a rise in the solid volume fraction of the nanoparticles increases the viscous forces of the nanofluid but the internal heating of the nanofluid due to the heat from the collision of the nanoparticles weaken the viscous forces thereby making the momentum boundary layer thicker.

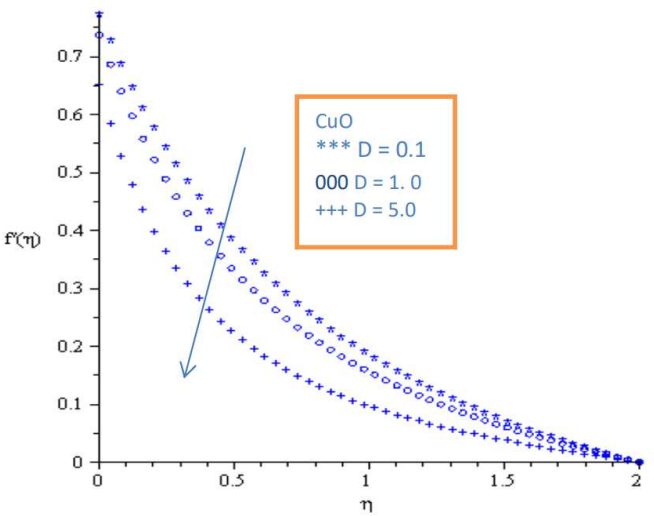

Figure 2: Velocity profile for varying values of local inertial coefficient for $Pr = 100, \varphi = 0.1, K^* = 0.1, H = 0.2, Ec = 0.1, L = 0.1, E = 0.1, \sigma = 0.1, \beta = 0.1, S = 0.1, N = 0.1$ and $M = 0.1$.

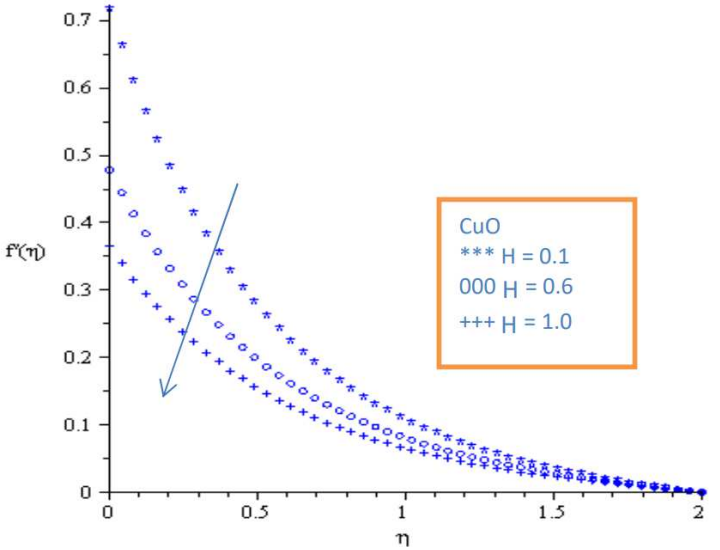

Figure 3: Velocity profile for varying values of velocity slip parameter for $Pr = 100$, $S = 1$, $D = 0.1$, $Ec = 0.1$, $\varphi = 0.1$, $L = 0.1$, $E = 0.1$, $\sigma = 0.1$, $\beta = 0.1$, $K^* = 0.1$, $N = 0.1$ and $M = 0.1$.

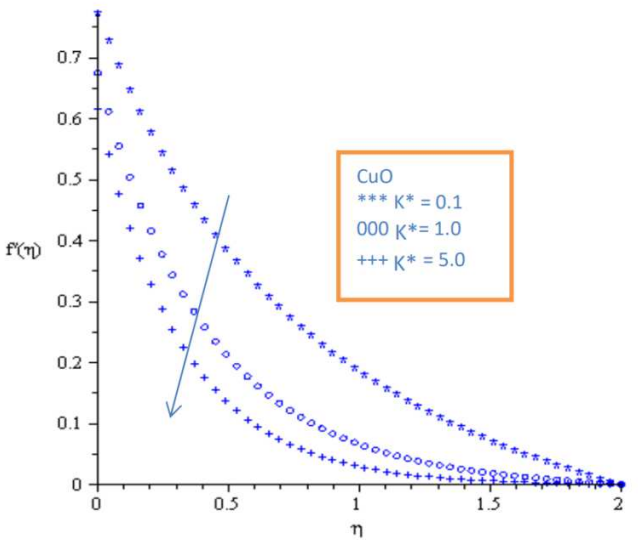

Figure 4: Velocity profile for varying values of permeability parameter for $Pr = 100, \varphi = 0.1, D = 0.1, Ec = 0.1, L = 0.1, H = 0.2, E = 0.1, \sigma = 0.1, \beta = 0.1, f = 0.1, N = 0.1$ and $M = 0.1$.

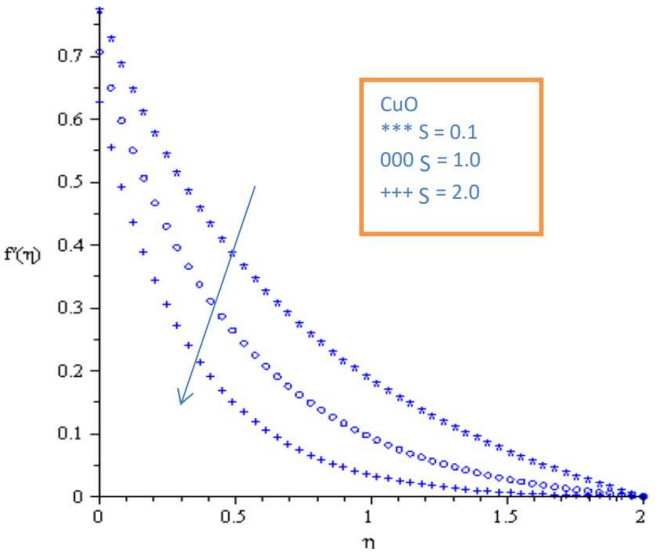

Figure 5: Velocity profile for varying values of suction parameter for $Pr = 100$, $\varphi = 0.1$, $D = 0.1$, $Ec = 0.1$, $L = 0.1$, $H = 0.2, E = 0.1, \sigma = 0.1, \beta = 0.1, K = 0.1, N = 0.1$ and $M = 0.1$.

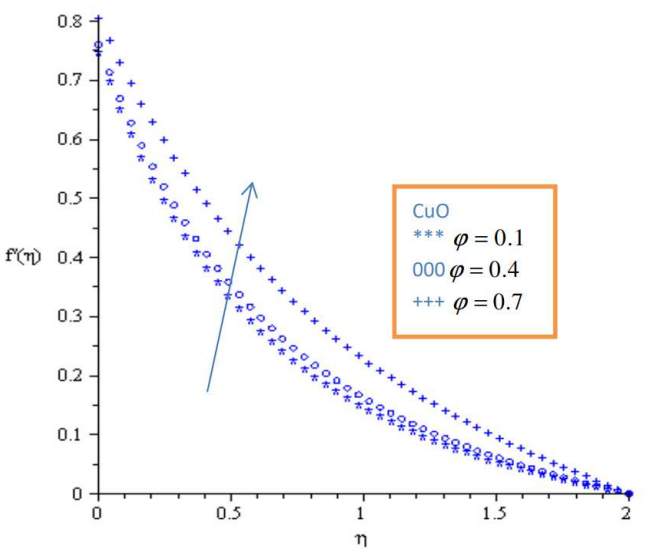

Figure 6: Velocity profile for varying values of solid volume fraction of nanoparticles for $Pr = 100$, $H = 0.2$, $D = 0.1$, $K^* = 0.5$, $Ec = 0.1$, $L = 0.2$, $E = 0.1$, $\sigma = 0.1$, $\beta = 0.1$, $S = 0.1$, $N = 0.1$ and $M = 0.1$

5.2. Temperature profiles

The thermal boundary layer profiles are depicted in Figures 7-14. Figure 7 highlights the effects of increasing the local inertial coefficient on the temperature field of the nanofluid within the boundary layer. An increase in the inertia coefficient increases the thermal boundary layer thickness. This is because a hike in the local inertial coefficient enhances the hydrodynamic dragging of CuO nanoparticles which increases the temperature of the nanofluid and subsequently thickening the thermal boundary layer.

The temperature profiles of Figures 8-10 exhibit similar trends as that of Figure 7 as the solid volume fraction of CuO nanoparticles, permeability parameter and Eckert number were increased. An appreciation of these parameters decays the boundary layer enthalpy difference which increases the temperature of the nanofluid and subsequently enhancing the thermal boundary layer thickness. But the velocity slip parameter is noted in Figure 11 to decrease the temperature of the nanofluid. The slip condition promotes the transfer of heat from the surface of the plate which deteriorates the thermal boundary layer thickness. The temperature profiles for the temperature jump parameter, Prandtl number and suction parameter depicted in Figures 12-14 present similar patterns as that of Figure 11. Increasing magnitudes of these parameters decay the thermal diffusivity of the nanofluid within the boundary layer and as a result makes the thermal boundary layer thinner.

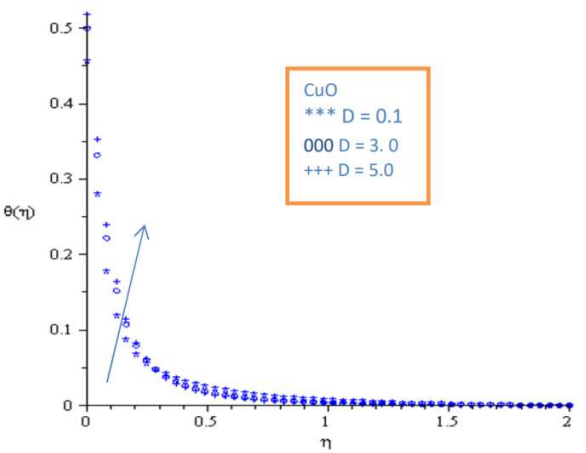

Figure 7: Temperature profile for varying values of local inertial coefficient for $Pr = 100, \varphi = 0.1, K^* = 0.1, Ec = 0.1, L = 0.1, E = 0.1, H = 0.2, \sigma = 0.1, \beta = 0.1, S = 0.1, N = 0.1$ and $M = 0.1$.

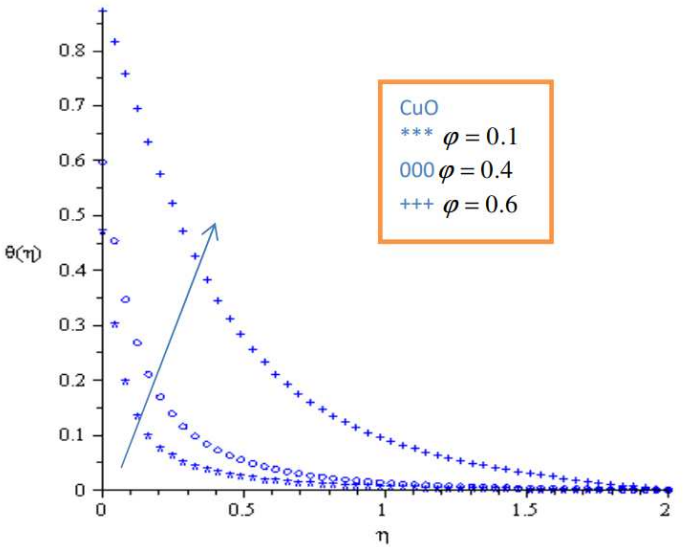

Figure 8: Temperature profile for varying values of solid volume fraction of nanoparticles for $Pr = 100, H = 0.2, D = 0.1, K^* = 0.5, Ec = 0.1, L = 0.2, E = 0.1, \sigma = 0.1, \beta = 0.1, S = 0.1, N = 0.1$ and $M = 0.1$

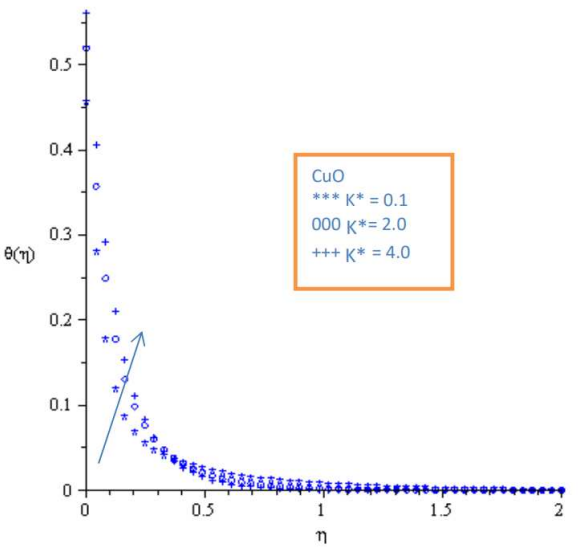

Figure 9: Temperature profile for varying values of permeability parameter for $Pr = 100, \varphi = 0.1, D = 0.1, Ec = 0.1, L = 0.1, H = 0.2, E = 0.1, \sigma = 0.1, \beta = 0.1, f = 0.1, N = 0.1$ and $M = 0.1$.

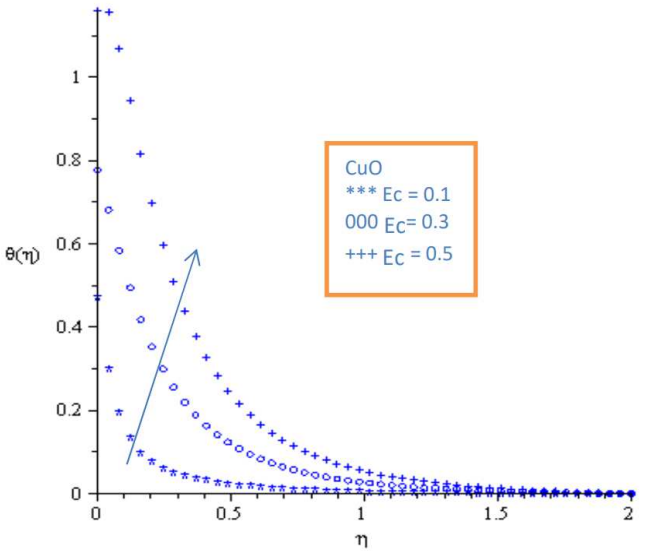

Figure 10: Temperature profile for varying values of Eckert number for $K^* = 0.1, \varphi = 0.1, D = 0.1, Pr = 100, L = 0.1, E = 0.1, H = 0.2, \sigma = 0.1,\ \beta = 0.1,\ S = 0.1,\ N = 0.1$ and $M = 0.1$.

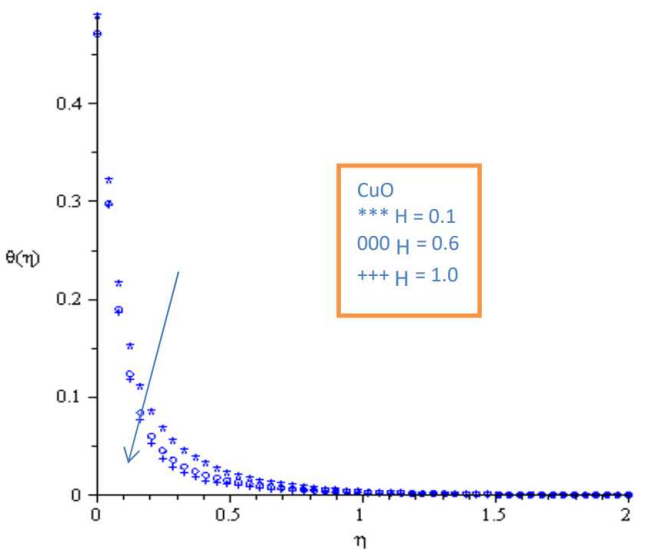

Figure 11: Temperature profile for varying values of velocity slip parameter for $Pr = 100, S = 1, D = 0.1, Ec = 0.1, \varphi = 0.1, L = 0.1, E = 0.1,\ \sigma = 0.1,\ H = 0.2,\ \beta = 0.1, K^* = 0.1, N = 0.1$ and $M = 0.1$.

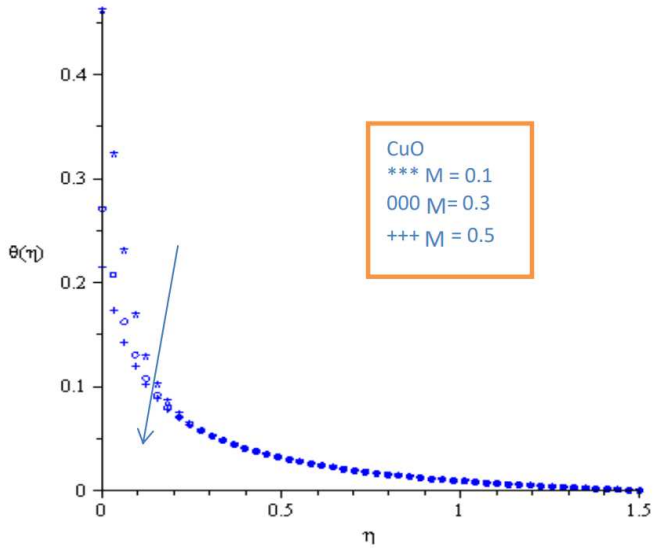

Figure 12: Temperature profile for varying values of temperature jump parameter for $K^* = 0.1, \varphi = 0.1, D = 0.1, Pr = 100, L = 0.1, E = 0.1, \sigma = 0.1, H = 0.2, \beta = 0.1, f = 0.1, N = 0.1$ and $Ec = 0.1$.

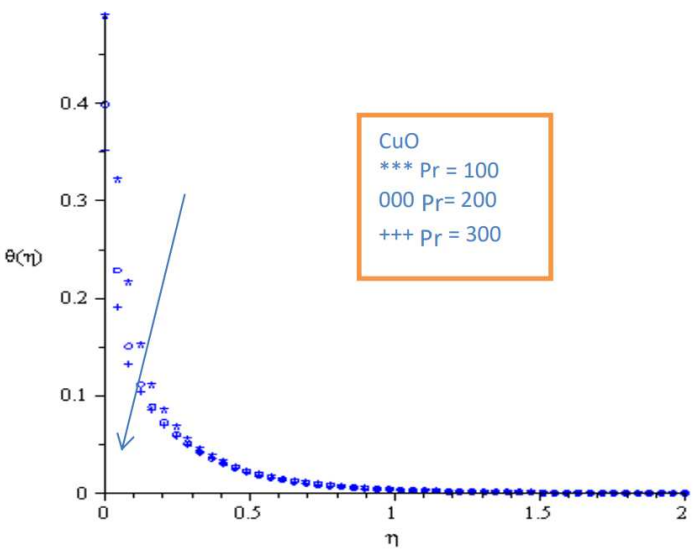

Figure 13: Temperature Profile for varying values of Prandtl number for $K^* = 1, \varphi = 0.1, D = 0.1, Ec = 0.1, L = 0.1, E = 0.1, H = 0.2,\ \sigma = 0.1,\ \beta = 0.1,\ f = 0.1,\ N = 0.1$ and $M = 0.1$.

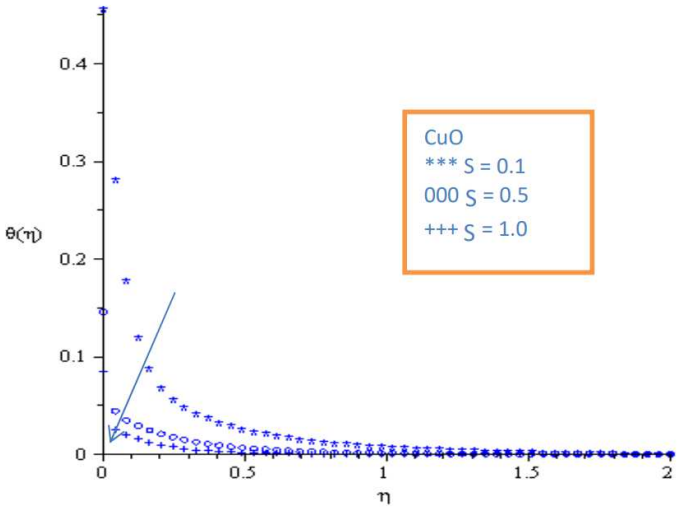

Figure 14: Temperature profile for varying values of suction parameter for $Pr = 100, \varphi = 0.1, D = 0.1, Ec = 0.1, L = 0.1, E = 0.1, \sigma = 0.1, H = 0.2, \beta = 0.1, K = 0.1, N = 0.1$ and $M = 0.1$.

5.3. Concentration profiles

The concentration profiles are presented in Figures 15-24. Figure 15 depicts the impact of the local inertial coefficient on the concentration profile. The local inertial coefficient is noted to increase the concentration of the nanofluid fluid within the boundary layer. This is can be attributed to the fact that an increase in the local inertial coefficient opposes mass diffusion of CuO nanoparticles from the surface of the plate due to the built-up resistive forces in the flow and as a result thickens the solutal boundary layer. The activation energy, velocity slip and permeability parameters illustrated in Figures 16-18 also enhance the solutal boundary thickness. This is because an increase in the activation energy, velocity slip and permeability parameters deplete the rate of mass diffusion across the boundary layer which enhances the concentration of the nanofluid. Contrarily, it is observed in Figure 19 that increasing the Lewis number decays the concentration of the nanofluid. Physically, an increase in the Lewis number enhances thermal diffusivity of CuO nanoparticles over its mass diffusivity, thereby degrading the solutal boundary layer thickness. The temperature difference parameter, fitted rate parameter, chemical reaction rate parameter, Prandtl number and suction parameter were seen in Figures 20-24 to also deplete the solutal boundary layer thickness due to enhanced mass diffusivity.

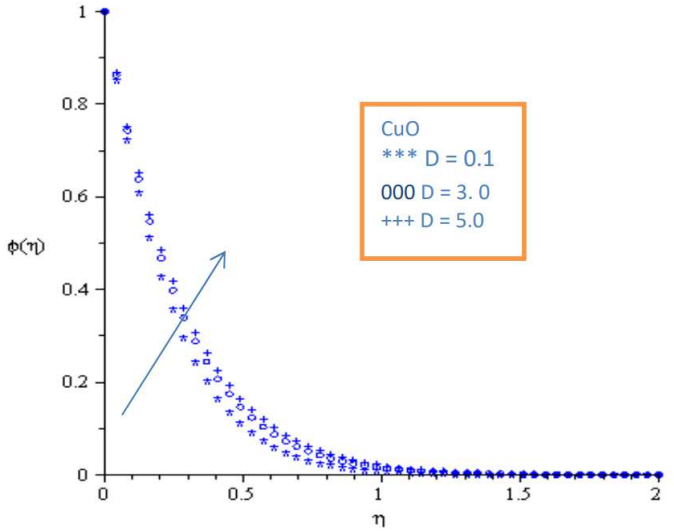

Figure 15: Concentration profile for varying values of local inertial coefficient for $Pr = 100, \varphi = 0.1, K^* = 0.1, Ec = 0.1, L = 0.1, E = 0.1, H = 0.2, \sigma = 0.1, \beta = 0.1, S = 0.1, N = 0.1$ and $M = 0.1$.

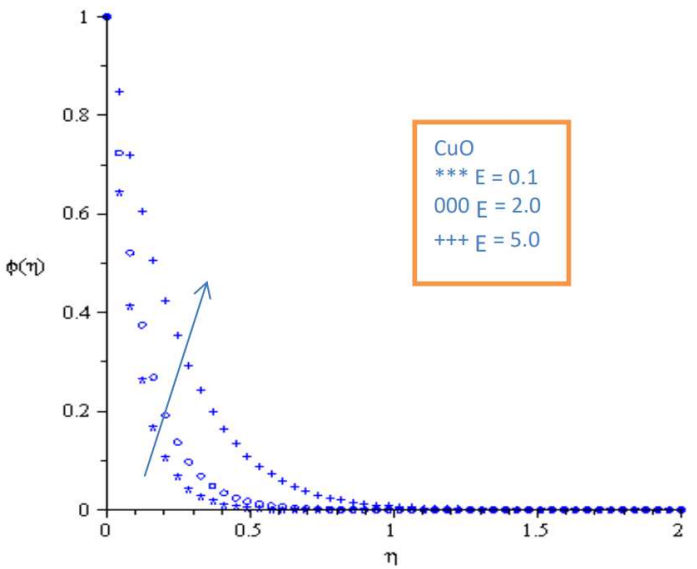

Figure 16: Concentration profile for varying values of activation energy for $Pr = 100, \varphi = 0.1, D = 0.1, Ec = 2, L = 0.1, S = 0.1, H = 0.2, \sigma = 0.1, \beta = 10, K = 0.1, N = 0.1$ and $M = 0.1$.

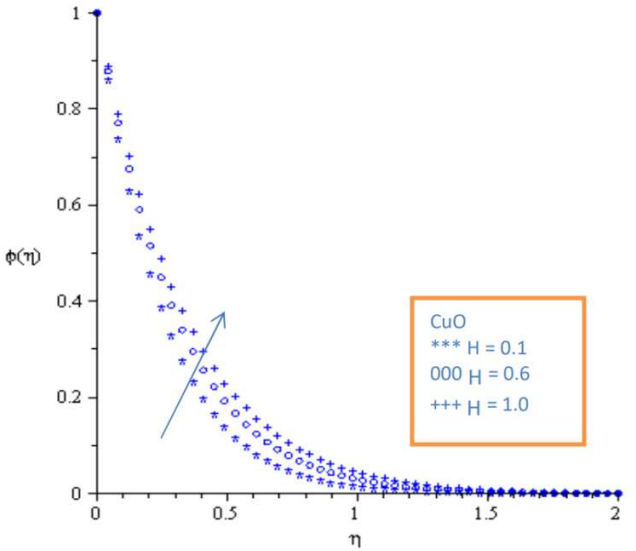

Figure 17: Concentration profile for varying values of velocity slip parameter for $Pr = 100,\quad S = 1, D = 0.1, Ec = 0.1, \varphi = 0.1, L = 0.1, E = 0.1, \sigma = 0.1, H = 0.2, \beta = 0.1, K^* = 0.1, N = 0.1$ and $M = 0.1$.

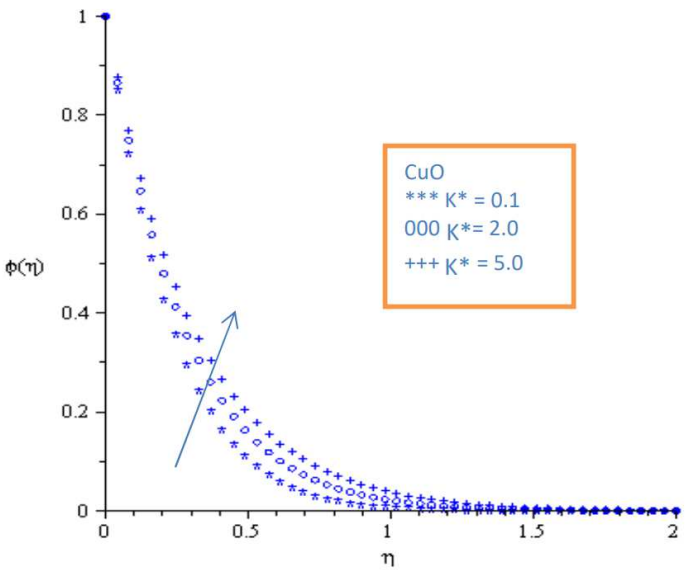

Figure 18: Concentration profile for varying values of permeability parameter for $Pr = 100, \varphi = 0.1, D = 0.1, Ec = 0.1, L = 0.1, H = 0.2, E = 0.1, \sigma = 0.1, \beta = 0.1, f = 0.1, N = 0.1$ and $M = 0.1$.

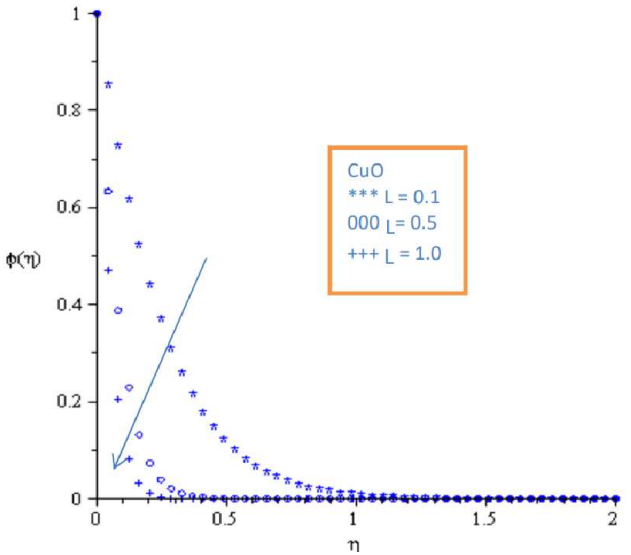

Figure 19: Concentration profile for varying values of Lewis number for $Pr = 100$, $\varphi = 0.1$, $D = 0.1, Ec = 0.1, S = 0.1, H = 0.2, E = 0.1, \sigma = 0.1$, $\beta = 0.1, K = 0.5, N = 0.1$ and $M = 0.1$.

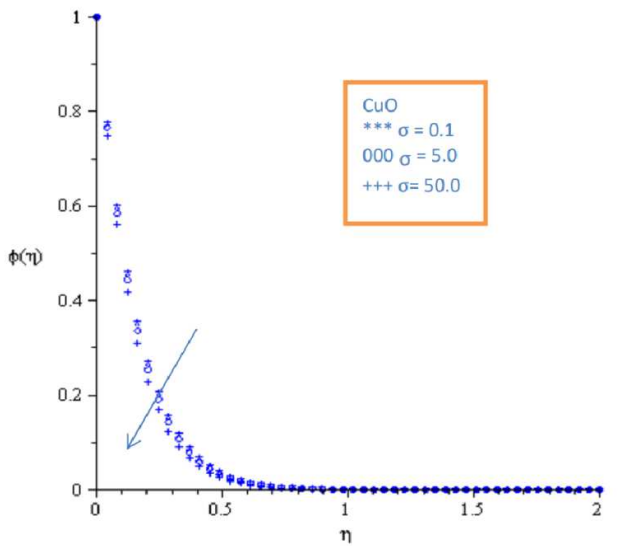

Figure 20: Concentration profile for varying values of temperature difference parameter for $Pr = 100, \varphi = 0.1, H = 0.2, D = 0.1, Ec = 2, E = 0.1, S = 0.1, \sigma = 0.1, \beta = 2, K = 0.1, N = 0.1$ and $M = 0.1$.

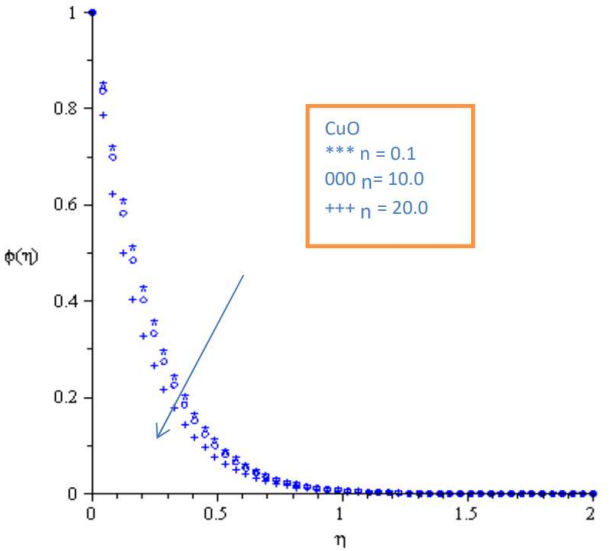

Figure 21: Concentration profile for varying values of fitted rate parameter for $Pr = 100$, $\varphi = 0.1, D = 0.1, Ec = 2, E = 0.1, H = 0.2, S = 0.1, \sigma = 0.1, \beta = 0.1, K = 0.1, N = 0.1$ and $M = 0.1$.

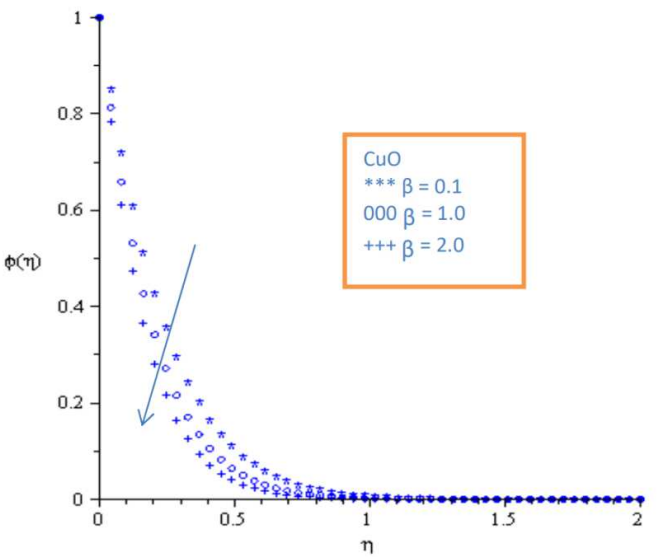

Figure 22: Concentration profile for varying values of chemical reaction rate parameter for $Pr = 100, \varphi = 0.1, \quad D = 0.1, H = 0.2, Ec = 2, E = 0.1, S = 0.1, L = 0.1, \sigma = 0.1,$ $K = 0.1, N = 0.1$ and $M = 0.1$.

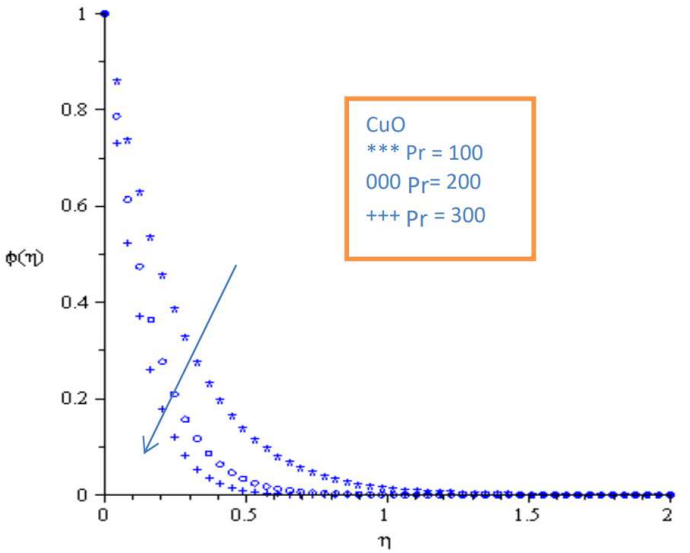

Figure 23: Concentration profile for varying values of Prandtl number for $K^* = 1$, $\varphi = 0.1$, $D = 0.1$, $Ec = 0.1$, $L = 0.1, E = 0.1, H = 0.2, \sigma = 0.1, \beta = 0.1, f = 0.1, N = 0.1$ and $M = 0.1$.

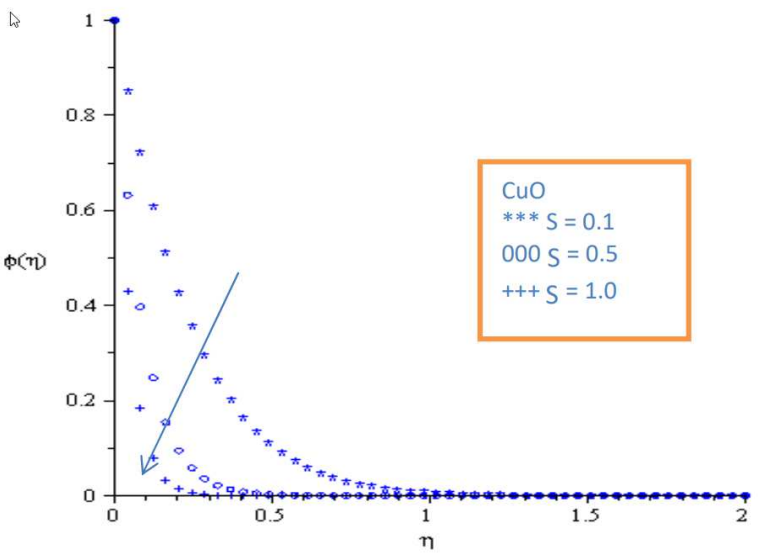

Figure 24: Concentration profile for varying values of suction parameter for $Pr = 100$, $\varphi = 0.1$, $D = 0.1$, $Ec = 0.1, L = 0.1, E = 0.1$, $\sigma = 0.1$, $H = 0.2, \beta = 0.1, K = 0.1, N = 0.1$ and $M = 0.1$.

6. Conclusions

The impact of fluctuating temperature on Darcy-Forchheimer flow of oil-based nanofluid with activation energy and velocity slip has been studied. The resulting coupled nonlinear ordinary differential equations governing the flow problem was solved numerically by employing the fourth order Runge-Kutta algorithm with a shooting method. Results for the entrenched parameters controlling the flow dynamics have been tabulated and illustrated graphically. The findings of the study are summarized as:

- The activation energy depleted the Sherwood number while the Lewis number, chemical reaction rate parameter and fitted rate parameter appreciated the Sherwood number.

- The temperature jump parameter degraded both the Nusselt and Sherwood numbers while the Prandtl number increased the intensities of both the Nusselt and Sherwood numbers.

- The velocity slip parameter, permeability parameter, suction parameter and local inertial coefficient deteriorated the momentum boundary layer thickness while the magnitude of the solid volume fraction of CuO nanoparticles enhanced the momentum boundary layer thickness.

- The solid volume fraction of CuO nanoparticles, permeability parameter, Eckert number and local inertial coefficient enhanced the thermal boundary layer thickness while the velocity slip parameter, temperature jump parameter, Prandtl number and suction parameter decayed the thermal boundary layer thickness.

- The local inertial coefficient, activation energy parameter, velocity slip parameter and permeability parameter enhanced the solutal boundary layer thickness while the Lewis number, temperature difference parameter, fitted rate parameter, chemical reaction rate parameter, Prandtl number and suction parameter weaken the solutal boundary layer thickness.

Conflict of Interest

There is no conflict of interest in this research.

Acknowledgement

The authors acknowledge the invaluable comments of all reviewers that contribute to sharpening the manuscript for consideration

References

[1] A. Mahdy and A.J. Chamkha, Chemical reaction and viscous dissipation effects on Darcy-Forchheimer mixed convection in a fluid saturated porous media, *Int. J. Num. Methods for Heat and Fluid Flow* 20(8) (2010), 924-940. https://doi.org/10.1108/09615531011081441

[2] N. Kishan and S. Maripala, Thermophoresis and viscous dissipation effects on Darcy-Forchheimer MHD mixed convection in a fluid saturated porous media, *Advances in Applied Science Research* 3(1) (2012), 60-74.

[3] N. Kishan and S. Jagadha, Thermophoresis and chemical reaction effects on MHD Darcy-Forchheimer mixed convection in a fluid saturated porous media, *International Journal of Engineering Trends and Technology* 10(5) (2014), 235-243. https://doi.org/10.14445/22315381/IJETT-V10P245

[4] S. Maripala and N. Kishan, Soret and Dufour effects on Darcy-Forchheimer MHD mixed convection in a fluid saturated porous media with viscous dissipation and Thermophoresis, *Elixir Appl. Math.* 81 (2015), 31863-31868.

[5] T. Sajid, M. Sagheer, S. Hussain and M. Bilal, Darcy-Forchheimer flow of Maxwell nanofluid flow with nonlinear thermal radiation and activation energy, *AIP Advances* 8 (2018), 1-19. https://doi.org/10.1063/1.5019218

[6] S. Jagadha and P. Amrutha, MHD boundary layer flow of Darcy-Forchheimer mixed convection in a nanofluid saturated porous media with viscous dissipation, *AAM Special Issue* 4 (2019), 117-134.

[7] G. Rasool and T. Zhang, Darcy-Forchheimer nanofluidic flow manifested with Cattaneo-Christov theory of heat and mass flux over non-linearly stretching surface, *PLoSONE* 14(8) (2019), e0221302. https://doi.org/10.1371/journal.pone.0221302

[8] M. Asma, W.A.M. Othman and T. Muhammad, Numerical study for Darcy-Forchheimer flow of nanofluid due to a rotating disk with binary chemical reaction and Arrhenius activation energy, *Mathematics* 7(10) (2019), 921. https://doi.org/10.3390/math7100921

[9] I. Uddin, R. Akhtar, Z. Zhiyu, S. Islam, M. Shoaib and M.A.Z. Raja, Numerical treatment for Darcy-Forchheimer flow of Sisko nanomaterial with nonlinear thermal radiation by Lobatto IIIA technique, *Mathematical Problems in Engineering* 2019 (2019), Article ID 8974572, 5 pp. https://doi.org/10.1155/2019/8974572

[10] G. Rasool, T. Zhang, A.J. Chamkha, A. Shafiq, I. Tlili and G. Shahzadi, Entropy generation and consequences of binary chemical reaction on MHD Darcy-Forchheimer Williamson nanofluid flow over non-linearly stretching surface, *Entropy* 22(18) (2020), 1- 21. https://doi.org/10.3390/e22010018

[11] M. Ramzan, N. Ullah, J.D. Chung, D. Lu and U. Farooq, Buoyancy effects on the radiative magneto Micropolar nanofluid flow with double stratification, activation energy and binary chemical reaction, *Scientific Reports* 7(12901) (2017), 1-15. https://doi.org/10.1038/s41598-017-13140-6

[12] S. Anuradha and M. Yegammai, MHD radiative boundary layer flow of nanofluid past a vertical plate with effects of binary chemical reaction and activation energy, *Global Journal of Pure and Applied Mathematics* 13(9) (2017), 6377-6392.

[13] R.V.M.S.S.K. Kumar, G.V. Kumar, C.S.K. Raju, S.A. Shehzad and. S.V.K. Varma, Analysis of Arrhenius activation energy in magnetohydrodynamic Carreau fluid flow through improved theory of heat diffusion and binary chemical reaction, *J. Phys. Commun.* 2 (2018), 035004. https://doi.org/10.1088/2399-6528/aaafff

[14] M. Asma, W.A.M. Othman and T. Muhammad, Numerical study for Darcy-Forchheimer flow of nanofluid due to a rotating disk with binary chemical reaction and Arrhenius activation energy, *Mathematics* 7(921) (2019), 1-17. https://doi.org/10.3390/math7100921

[15] M. Ijaz, M. Ayub and H. Khan, Entropy generation and activation energy mechanism in nonlinear radiative flow of Sisko nanofluid: rotating disk, *Heliyon* 5 (2019), 1-12. https://doi.org/10.1016/j.heliyon.2019.e01863

[16] M. Dhlamini, P.K. Kameswaran, P. Sibanda, S. Motsa and H. Mondal, Activation energy and binary chemical reaction effects in mixed convective nanofluid flow with convective boundary conditions, *Journal of Computational Design and Engineering* 6 (2019), 149-158. https://doi.org/10.1016/j.jcde.2018.07.002

[17] M. Dhlamini, H. Mondal, P. Sibanda and S. Motsa, Activation energy and entropy generation in viscous nanofluid with higher order chemically reacting species, *International Journal of Ambient Energy* 43 (2020), 1495-1507. https://doi.org/10.1080/01430750.2019.1710564

[18] M.M. Rashidi and N.F. Mehr, Effects of velocity slip and temperature jump on the entropy generation in magnetohydrodynamic flow over a porous rotating disk, *Journal of Mechanical Engineering* 1(3) (2012), 4-14.

[19] G. Singh and O.D. Makinde, Mixed convection slip flow with temperature jump along a moving plate in presence of free stream, *Thermal Science* 19(1) (2015), 119-128. https://doi.org/10.2298/TSCI120718110S

[20] S.O. Adesanya, Free convective flow of heat generating fluid through a porous vertical channel with velocity slip and temperature jump, *Ain Shams Engineering Journal* 6 (2015), 1045-1052. https://doi.org/10.1016/j.asej.2014.12.008

[21] K. Vajravelu, S. Sreenadh and R. Saravana, Influence of velocity slip and temperature jump conditions on the peristaltic flow of a Jeffrey fluid in contact with a Newtonian fluid, *Applied Mathematics and Nonlinear Sciences* 2(2) (2017), 429-442. https://doi.org/10.21042/AMNS.2017.2.00034

[22] A.A. Opanuga, O.O. Agboola, H.I. Okagbue and A.M. Olanrewaju, Hall current and ion-slip effects on the entropy generation of couple stress fluid with velocity slip and temperature jump, *International Journal of Mechanics* 12 (2018), 221-231.

[23] E.O. Titiloye, J.A. Gbadeyan and A.T. Adeosun, An oscillatory radiating hydromagnetic internal heat generating fluid flow through a vertical porous channel with slip and temperature jump, *Int. J. of Applied Mechanics and Engineering* 23(2) (2018), 503-519. https://doi.org/10.2478/ijame-2018-0029

[24] K. Gangadhar, K.V. Ramana and B.R. Kumar, Velocity slip and thermal jump on Maxwell fluid with non-Fourier Cattaneo-Christov heat flux using SRM solutions, *Int. J. Eng. and Tech.* 7(4.10) (2018), 233-239. https://doi.org/10.14419/ijet.v7i4.10.20902

[25] F. Almutairi, S.M. Khaled and A. Ebaid, MHD flow of nanofluid with homogeneous-heterogeneous reactions in a porous medium under the influence of second-order velocity slip, *Mathematics* 7(220) (2019), 1-11. https://doi.org/10.3390/math7030220

[26] J. Zhu, Y. Xu and X. Han, A non-Newtonian magnetohydrodynamics (MHD) nanofluid flow and heat transfer with nonlinear slip and temperature jump, *Mathematics* 7(1199) (2019), 1-21. https://doi.org/10.3390/math7121199

[27] C.J. Etwire, I.Y. Seini, M. Rabiu and O.D. Makinde, Impact of thermophoretic transport of Al2O3 nanoparticles on viscoelastic flow of oil-based nanofluid over a porous exponentially stretching surface with activation energy, *Engineering Transactions* 67(3) (2019), 387-410.

[28] C.J. Etwire, I.Y. Seini, M. Rabiu and O.D. Makinde, Effects of viscoelastic oil-based nanofluids on a porous nonlinear stretching surface with variable heat source/sink, *Defect and Diffusion Forum-Computational Analysis of Heat Transfer in Fluids and Solids* 387 (2018), 260-272. https://doi.org/10.4028/www.scientific.net/DDF.387.260

[29] C.J. Etwire, I.Y. Seini, M. Rabiu and O.D. Makinde, Combined effects of variable viscosity and thermal conductivity on dissipative flow of oil-based nanofluid over a permeable vertical surface, *Diffusion Foundations* 16 (2018), 158-176. https://doi.org/10.4028/www.scientific.net/DF.16.158

[30] J.C. Maxwell, *A Treatise on Electricity and Magnetism*, UK: Clarendon, 1973.

[31] C.Y. Wang, Free convection on a vertical stretching surface, *Journal of Applied Mathematics and Mechanics/Zeitschriftfur Angewandte Mathematik und Mechanik* 69(11) (1989), 418-420. https://doi.org/10.1002/zamm.19890691115

[32] B. Bidin and R. Nazar, Numerical solution of the boundary layer flow over an exponentially stretching sheet with thermal radiation, *European Journal of Scientific Research* 33(4) (2009), 710-717.